RESEARCH
ENGINEERING
PRODUCTION

FOURTH
SEMIANNUAL TECHNICAL
SUMMARY REPORT

By   Manlio Abele
     Hector Medecki
     Joseph Tomagno
     Roger Tomboulian

ASTIA

APR 3 0 1963

TISIA   A

April 12, 1963

GENERAL APPLIED SCIENCE LABORATORIES, INC

ARPA ORDER No. 207-62
Contract No. Nonr 3475(00)

Period: September 16, 1962 to April 15, 1963

Title of Project

"Studies of the Electromagnetic Properties of Nonuniform Plasmas"

Prepared for

Director
Advanced Research Projects Agency
Department of Defense
Washington 25, D. C.

Prepared by

General Applied Science Laboratories, Inc.
Merrick and Stewart Avenues
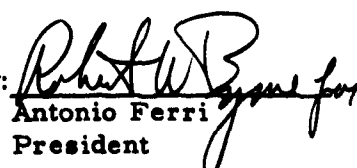Westbury, L. I., New York

April 12, 1963   Approved by: _____
                                      Antonio Ferri
                                      President

TABLE OF CONTENTS

I.   <u>INTRODUCTION</u>

This report will discuss the experimental arrangement for generating an axially nonuniform plasma in a shock tube and the preliminary data obtained from the microwave measurements in such a medium. The quantative interpretation of the data is being conducted at the present time. Some of the properties which are evident from the preliminary analysis of the experimental results will be discussed in the following sections.

Furthermore the report presents the numerical calculations of the flow field in the shock tube with a nonuniform temperature distribution in the driven section. The preliminary theoretical analysis of this propagation of a microwave signal in the nonuniform plasma will be presented.

II. THEORETICAL FLUID DYNAMIC AND ELECTROMAGNETIC ANALYSES FOR A NONUNIFORM MEDIUM

A. Interaction of a Shock Wave with an Interface or Contact Discontinuity

Contact discontinuities can occur between gases of different properties, for example, when two dissimilar gases exist side by side as in a shock tube, or when a portion of a gas has been heated so that its density is considerably different from the neighboring gas. This section is devoted to the interaction of a shock wave and a contact discontinuity of the latter type.

In the analysis of a shock wave propagating through a discontinuity interface, it can be shown that the reflected wave is either a shock or a rarefaction wave. In addition to this, the shock is partially transmitted in the second region. The general procedure followed in order to analyze the physical state after the interaction process is discussed below.

In Fig. II.1.1, S_i represents the incident shock wave, traveling toward the interface I between the region (0) and (4) of the driven gas at the same pressure, and temperature condition $T_4 > T_o$. Fig. II 1.2 presents the two possible configurations which correspond either to a reflected shock S_r or an exponent wave R_r · S_t denotes the transmitted shock.

The state of the gas in (3) and (0) remains the same but in the region between reflected and transmitted waves, the gas is set in motion. In general in this region an interface I is found between two regions at the same pressure and velocity. In Fig. II.1.2, the pressure in each state is plotted against particle velocity.

Fig. II.1 Interaction of a shock wave with an interface or contact discontinuity
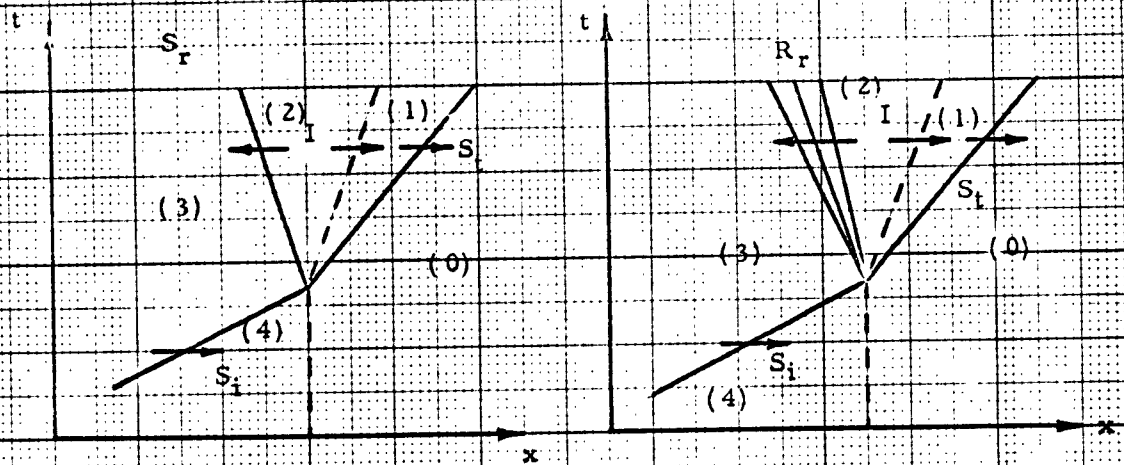

Fig. II.1.1 Before interaction

Fig. II.1.2 After interaction — (1) Reflected shock (2) Expansion wave
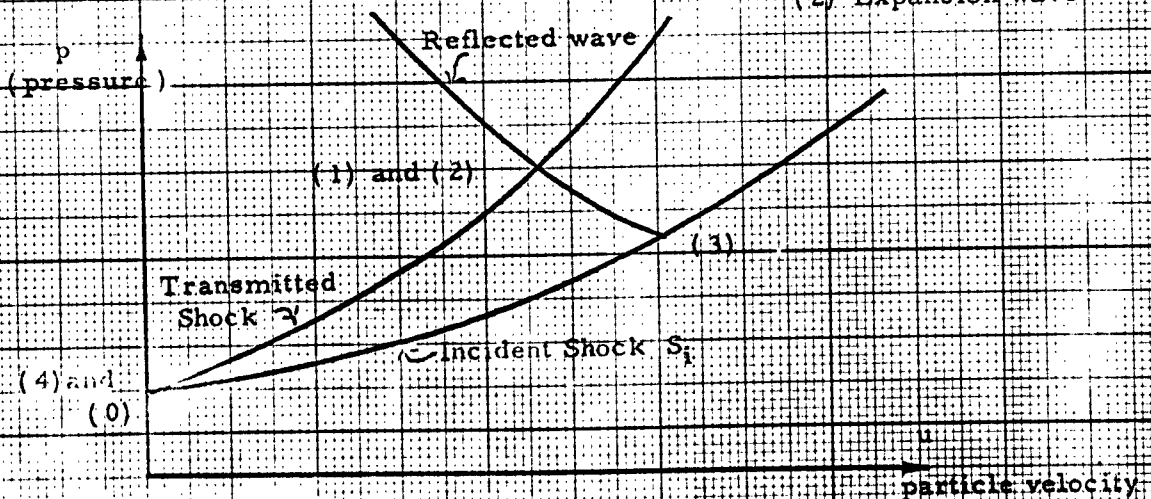
Fig. II.1.3 Particle velocity — pressure plot

GASL
Westbury, N.Y.

Because in (4) and (0) the gas is at rest and at the same pressure, both regions are represented by the same point in particle velocity - pressure (u , p) diagram. The disturbed left region (3) is connected to the undisturbed region of the first medium (4) through a normal shock and the curve (3) - (4) represents all the possible states that can be connected to (4) by means of a normal shock wave traveling to the right in a medium at rest. The state of the gas behind the incident normal shock has been computed using the equations derived from the conservation of mass, momentum and energy, considering real gas effects.

In Fig. II.1.3, the curve (1) - (0) represents the totality of states that can be connected to the second medium through a normal shock. It can be seen that if the curve (3) - (4) lies below (0) - (1), the state of the gas in region (3) can be connected to a state (2) only by means of a shock wave since the pressure at (2) is greater than at (3), hence the reflected wave is a shock. If the curve (3) - (0) lies above the curve (1) - (0), both states can be connected only by means of an expansion wave.

For cases where an adiabatic exponent can be introduced, it can easily be proved that if $\gamma_4 = \gamma_0$ one obtains either a reflected shock or an expansion wave depending upon whether $\rho_4 \overset{<}{>} \rho_0$ respectively. For the particular type of problems of interest, the transition between regions (2) and (3) occurs through a reflected shock.

B. Interaction of a Shock Wave with a Region with a Finite Gradient in Temperature

Assume now that the transition from medium (4) (hot gas) to medium (0) (cold gas) occurs through a region of length L with a finite gradient of temperature, at constant pressure. This assumption is consistent with a physical temperature distribution which can be obtained in the shock tube. For this case the flow field calculations have been performed assuming a constant temperature gradient over the length L (see Fig. II. 2.1).

The equation of motion in the region behind the shock is:

$$\left.\begin{array}{l} \rho u_t + \rho u u_x + p_x = 0 \\[2mm] \rho_t + \rho u_x + u\rho_x = 0 \\[2mm] p_t + u p_x - a^2 (\rho_t + u\rho_x) = 0 \end{array}\right\} \tag{1}$$

where ρ is the density, u the velocity of the particles, p the pressure, a, the speed of sound and t the time. These equations are formally the same if ρ is scaled to ρ_o, p to p_o, u and a to $\sqrt{RT_o}$, x to L and t to $\dfrac{L}{\sqrt{RT_o}}$.

It is well known that the system of differential equations governing a one dimensional non-isentropic flow (Ref. 4), is totally hyperbolic. Thus one obtains three real and distinct characteristics which are defined as follows:

Fig. II.2 Interaction of a shock wave with a region of a finite gradient of temperature

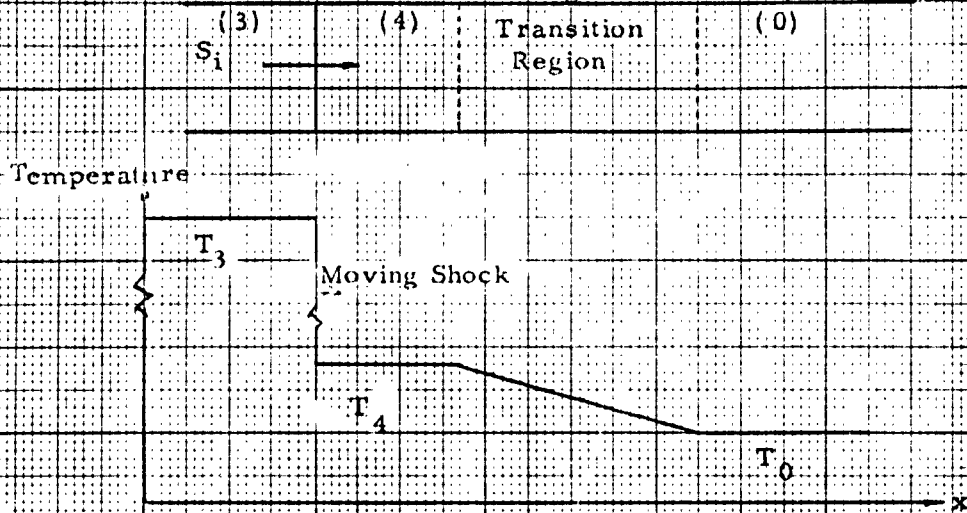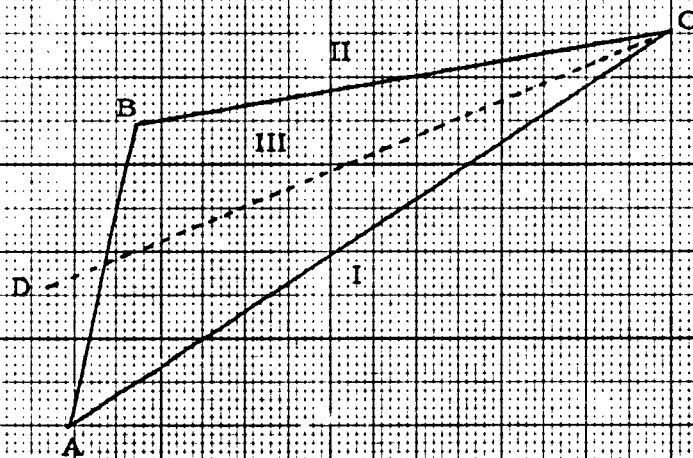Fig. II.2.1
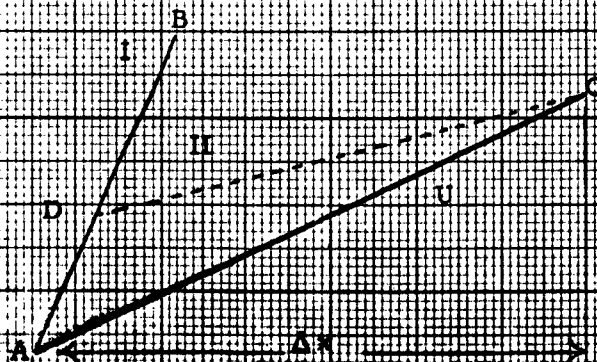

Fig. II.2.2 Characteristics and Streamline x-t plane

Fig. II.2.3 Intersection of characteristic and shock wave

$$I) \quad \frac{dx}{dt} = u - a$$

$$II) \quad \frac{dx}{dt} = u + a \tag{2}$$

$$III) \quad \frac{dx}{dt} = u$$

With reference to these three directions, the system of differential equations (1) has the form

$$p_I - a \rho u_I = 0$$

$$p_{II} + a \rho u_{II} = 0 \tag{3}$$

$$p_{III} - \rho h_{III} = 0$$

respective to I, II and III above.

In these equations, the subscripts mean differentiation along the characteristic direction (the enthalpy h has been scaled to RT_o).

The real gas effects have been considered in the numerical computations with the simplifying assumption of chemical equilibrium. Once p and h have been determined at C, (Fig. II. 2. 2), ρ, a, S and T can be computed at C by means of a special subroutine described in Ref. 6.

The shape of the transmitted shock wave traveling to the right is determined as follows: (Fig. II. 2. 3) if U is the shock wave velocity, scaled to $\sqrt{RT_o}$ and an index N indicates values in the region at rest in front of the

traveling shock the fundamental equations are:

$$\frac{\rho}{\rho_N} \qquad \frac{U}{U - u}$$

$$p - p_N = \rho_N U^2 (1 - \frac{\rho}{\rho_N}) \qquad (4)$$

$$h - h_N = \frac{1}{2} (p - p_N) (\frac{1}{\rho_N} + \frac{1}{\rho})$$

where symbols without indexes mean values at point C behind the shock wave.

The length L of variable temperature ahead of the shock is divided into N intervals. Then $\Delta x = L/N$, and in each interval Δx constant properties of the gas are assumed.

The shock velocity at A being known, the location of point C can be determined at a distance Δx. The physical parameters of the flow at C behind the shock wave can also be determined if the state of the gas is given along the I-characteristic originating from A.

Once the point D has been computed by using a backwards interpolation technique, the second equation of (3) is valid between C and D and together with the Mollier subroutine, provides the required information at C, considering C as a point located immediately behind the shock wave. Then the unknown shock wave velocity U at C is calculated from the system of equations (4).

A comparison between the above calculation using a finite temperature gradient and the calculation assuming a step change in temperature is presented in Fig. II.3.

C. Preliminary Theoretical Analysis of the Propagation of Electromagnetic Radiation into a Nonuniform Plasma

The propagation constant k, as defined from the equation

$$\frac{d^2E}{dx^2} + k^2E = 0$$

can be written in terms of the plasma frequency and collision frequency as:

$$k = \sqrt{\frac{\omega^2}{C^2}\left[1 - \frac{\omega_p^2}{\omega^2}\frac{1}{\left(1 - i\frac{\nu}{\omega}\right)}\right] - \gamma^2}$$

where γ is the root of the Bessel function divided by the tube radius for the TE_{11} circular waveguide mode. The propagation constant k can be written as,
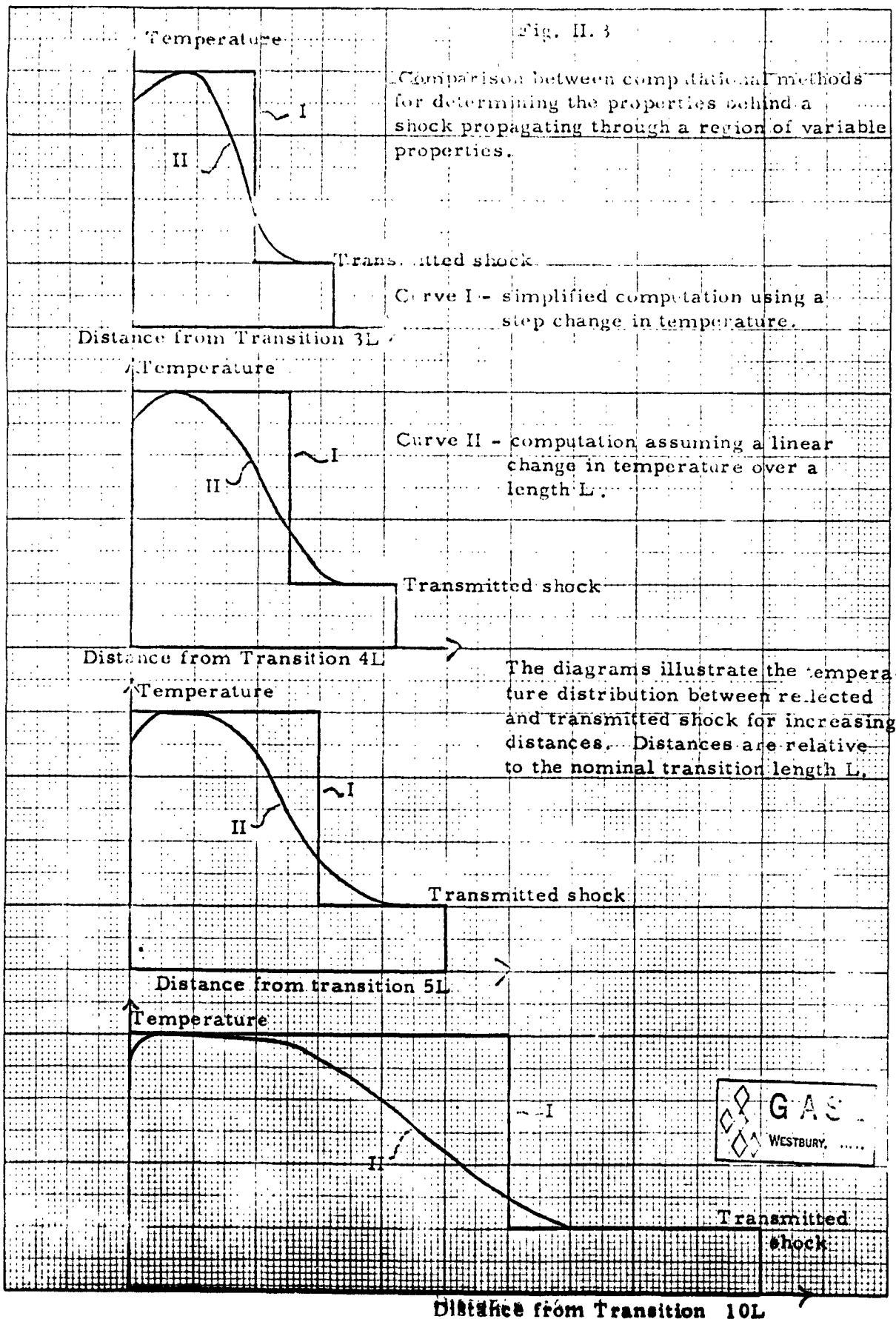
$$k = k_o K_g$$

with

$$k_o = \sqrt{\frac{\omega^2}{C^2} - \gamma^2}$$

$$K_g = \sqrt{1 - \frac{\omega_p^2}{C^2k_o^2}\frac{1}{\left(1 - i\frac{\nu}{\omega}\right)}}$$

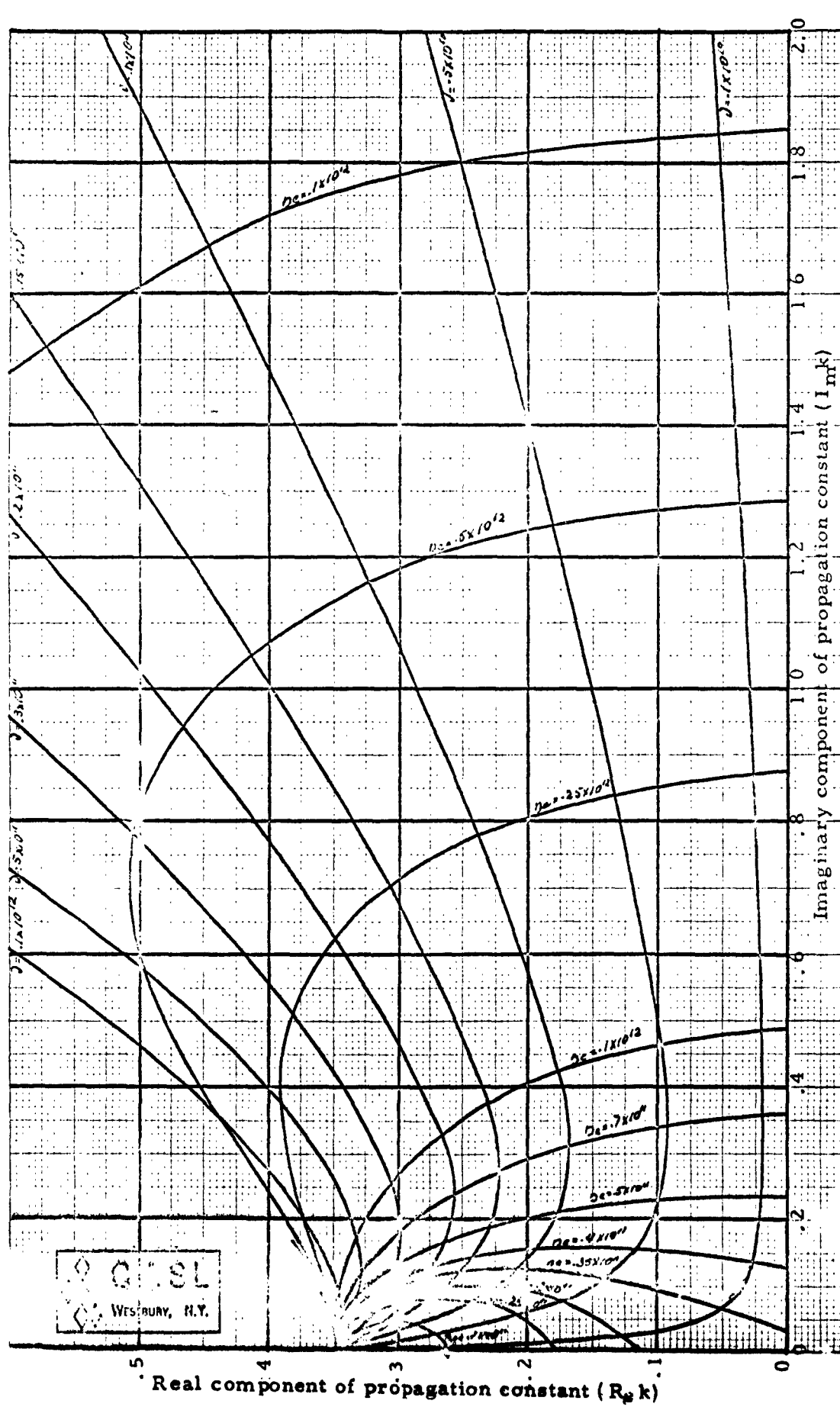where $\omega_p = 5.64 \times 10^4 \sqrt{n_e}$

The real and imaginary components of k are plotted in Fig. II.4 as a function of the electron density and collision frequency for $\lambda_g = 18.0$ cm.

Fig. II. 3

Comparison between computational methods for determining the properties behind a shock propagating through a region of variable properties.

Curve I - simplified computation using a step change in temperature.

Curve II - computation assuming a linear change in temperature over a length L.

The diagrams illustrate the temperature distribution between reflected and transmitted shock for increasing distances. Distances are relative to the nominal transition length L.

Real component of propagation constant ($R_e k$)

Imaginary component of propagation constant ($I_m k$)

Fig. II 4 Real and imaginary components of the propagation constant for $\gamma = .497$, $\lambda_g = 18.0$ cm, plotted for constant n_e and constant ν_i

Propagation from a Free Space Region into a Uniform Plasma Region

Let the radial electric field and tangential magnetic field in the free space region be given by,

$$E_r = A_o^1 \, e^{-ik_o x} \quad + \quad A_o^2 e^{ik_o x}$$

$$H_\theta = k_o \, \sqrt{\frac{\epsilon_o}{N_o}} \left[A_o^1 e^{-ik_o x} \, - A_o^2 \, e^{ik_o x} \right]$$

and in the region of uniform plasma

$$E_r = A_1^1 \, e^{-ik_1 x}$$

$$H_\theta = k_1 \sqrt{\frac{\epsilon_o}{N_o}} \left[A_1^1 \, e^{-ik_1 x} \right]$$

Matching boundary condition and letting $A_o^1 \equiv 1$,

$$E_r = e^{-ik_o x} + \beta \, e^{ik_o x}$$

where

$$\beta = \frac{1 - K_{g1}}{1 + K_{g1}} \quad \text{and } K_g \text{ is defined above.}$$

Hence,

$$E_r E_r^* = 1 + \beta \beta^* + \beta \, e^{-ik_o x} \, \beta^* \, e^{ik_o x}$$

where k_o is defined above.

This reduces to,

$$E_r E_r^* = \left[1 \pm \sqrt{(R_e \beta)^2 + (I_m \beta)^2} \right]^2$$

where the plus and minus indicate maximum and minimum values.

Thus,

$$SWR = \left[\frac{1 + \sqrt{(R_e \beta)^2 + (I_m \beta)^2}}{1 - \sqrt{(R_e \beta)^2 + (I_m \beta)^2}} \right]^2$$

The above equation has been programmed for the CDC computer in terms of the electron density and collision frequency. Typical curves are shown in Fig. III. 3.

Propagation from the Free Space Region into a Step-wise Changing Plasma Region

The model for the following calculation is presented below.
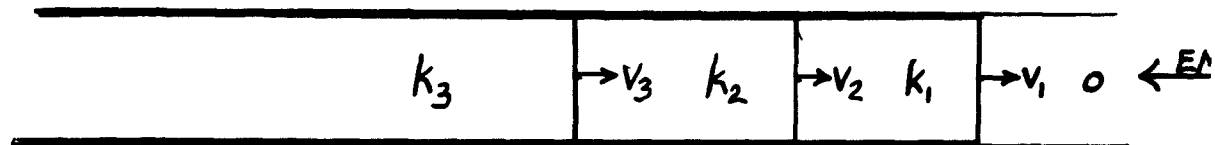
Here the free space region is characterized by subscripts O, and the plasma regions by 1, 2, and 3. The electric and magnetic field equation can be written as before and by matching boundary conditions the following set of equations is obtained:

$$A_1^0 e^{-ik_0 z_1} + A_2^0 e^{ik_0 z_1} = A_1^1 e^{-ik_1 z_1} + A_2^1 e^{ik_1 z_1}$$

$$k_0 \left[A_1^0 e^{-ik_0 z_1} - A_2^0 e^{ik z_1} \right] = k_1 \left[A_1^1 e^{-ik_1 z_1} - A_2^1 e^{ik_1 z_1} \right]$$

$$A_1^1 e^{ik_1 z_2} + A_2^1 e^{ik_1 z_2} = A_1^2 e^{-ik_2 z_2} + A_2^2 e^{ik_2 z_2}$$

$$k_1 \left[A_1^1 e^{-ik_1 z_2} - A_2^1 e^{ik_1 z_2} \right] = k_2 \left[A_1^2 e^{-ik_2 z_2} - A_2^2 e^{ik_2 z_2} \right]$$

$$A_1^2 e^{-ik_2 z_3} + A_2^2 e^{ik_2 z_3} = A_1^3 e^{-ik_3 z_3}$$

$$k_2 \left[A_1^2 e^{-ik_2 z_3} - A_2^2 e^{ik_2 z_3} \right] = k_3 \left[A_1^3 e^{-ik_3 z_3} \right]$$

In choosing the root of k, the $I_m k < 0$. The above set of equations has been programmed for the 7090 computer in terms of the electron densities, plasma frequencies and velocities of each region. This program has been used to compute the standing wave pattern for the idealized plasma configuration resulting from the calculations in Section II. A.

III. EXPERIMENTAL RESULTS

A. Uniform Plasma

At the onset of the air plasma measurements it was deemed essential to first measure the range of electron densities which can be obtained in the shock tube facility. It was found that sufficiently high electron densities ($n_e > 10^{11}$ e/cc) can be obtained at the test section by increasing the temperature of the hydrogen in the driver to 475°K and the driver pressure to 17 atmospheres. The equilibrium electron density of the plasma behind the shock at the test section can be computed by using standard tables in terms of the shock velocity and initial pressure in the driven section. An experimental curve of shock velocity vs. initial driven pressure for the above stated driver conditions is shown in Fig. III.1. The velocity is measured directly from the reflected microwave signal. In these measurements the temperature of the driven gas is kept uniform at room conditions.

In the plasma the electron density increases with the temperature at constant gas density and decreases with the gas density at constant temperature. For the experimental conditions encountered in the present measurement the change of electron density is relatively small over a rather extended range of shock velocities with constant driver gas conditions. This is apparent from Fig. III.2 where the change in electron density is within a factor of 3 over the range of velocities from 3000 to 4000 meters per second. The critical electron density for total microwave reflection ($n_e \approx 3.0 \times 10^{10}$ e/cc), is indicated and the corresponding shock velocity is 3470 meters per second.
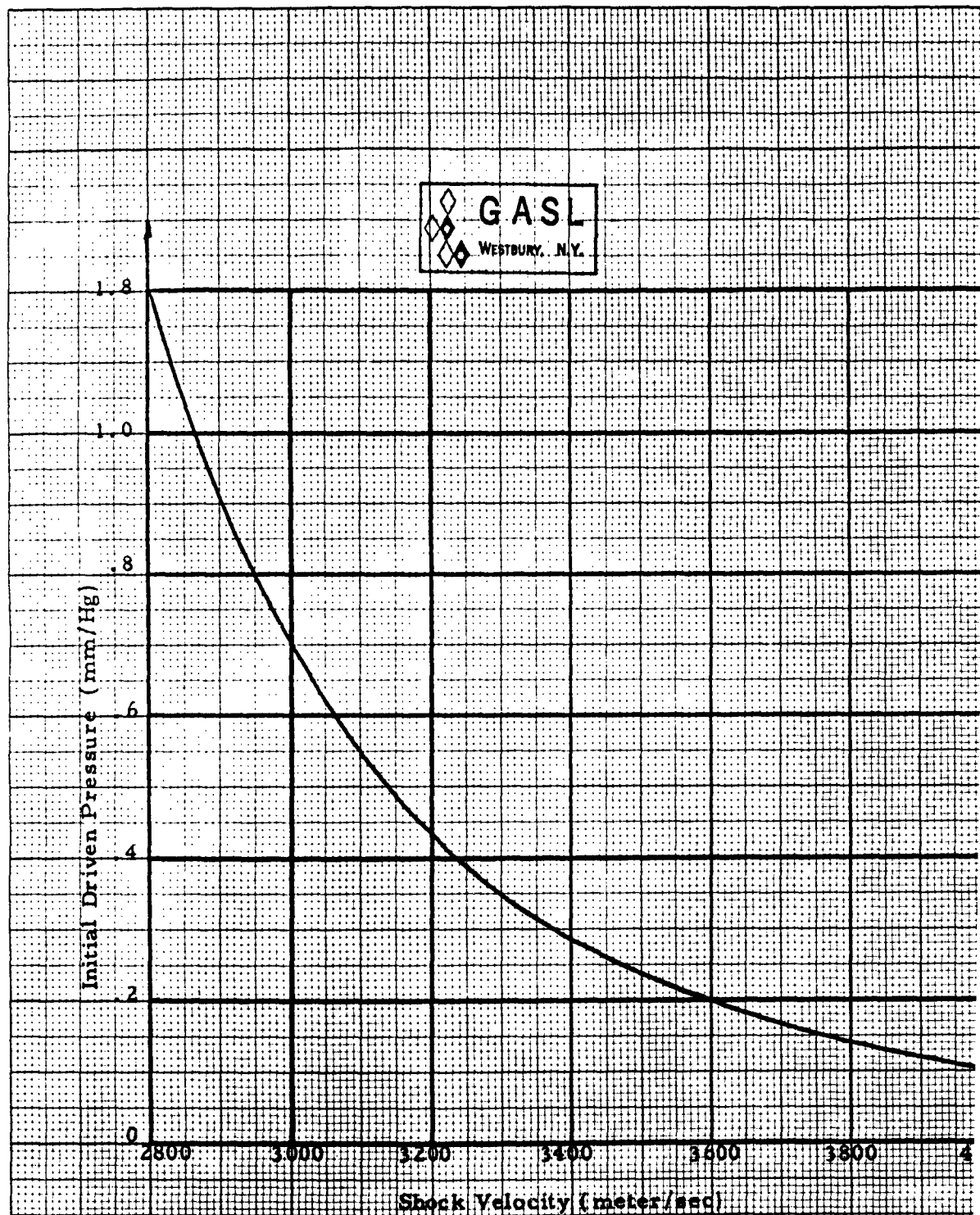
Figure III 1   Operating curve for uniform driven tube temperature (300°K)

Fig. III-2   Electron Density and Collision Frequency vs Shock Velocity for the Uniform Plasma Case
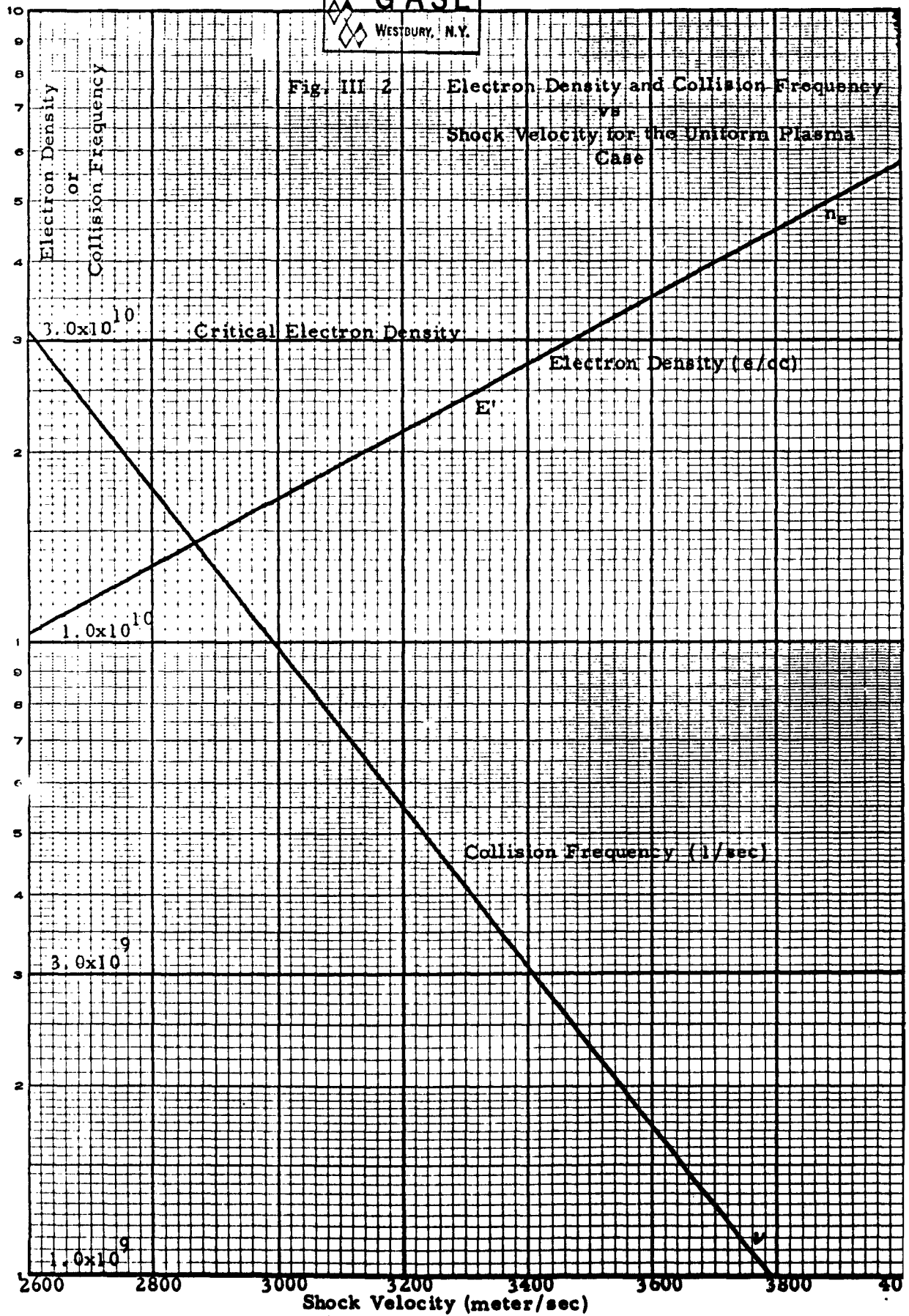
For the above operating conditions of the shock tube the calculated electron density level at a given shock velocity is strongly influenced by the initial conditions of the air in the driven section among other factors. The standing wave ratio of the reflected microwave radiation becomes a critical function of the electron density in the neighborhood of the total reflection condition. This property is apparent in Fig. III.3 where the theoretical standing wave ratio is computed (using the equations of Section II-C) for a uniform plasma in terms of shock velocity in the range of the present experimental conditions. Fig. III.3 is plotted with the collision frequency as a variable parameter. The calculated value of collision frequency is plotted in Fig. III.2.

As stated above, slight perturbations of the operating conditions (due to changes in driven temperature, rate of initial shock formation, varying shock attenuation and impurities) may produce a large scattering of the experimental results in the neighborhood of the shock velocity at which the critical electron density is attained. A pair of pictures is presented in Fig. III.4 representing the standing wave pattern below and above the critical velocity. The real significance of these pictures is the large change of the standing wave ratio obtained with a small change in shock velocity in the vicinity of the critical value.

In the pictures in Fig. III.4 a blanking signal is apparent on the trace. The start of the blanked portion corresponds to the arrival of the shock front at the position of the field detector. The distance from this marker to the last maximum in the magnetic field trace corresponds to the
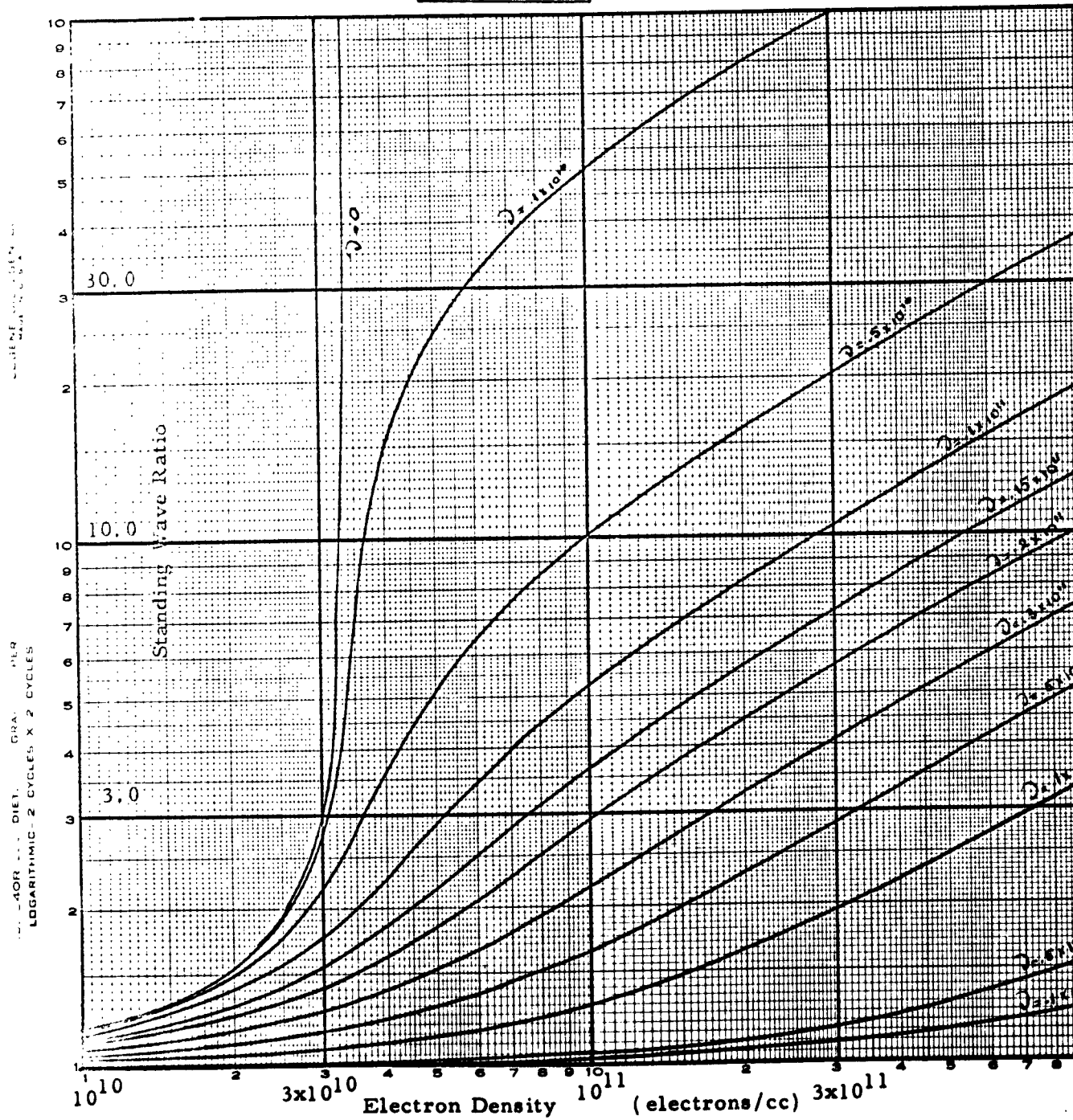
Fig. III 3   Calculated standing wave ratio as a function of
electron density (for various values of collision frequency (ν).
$\gamma = .497$ $\lambda_g = 18.0$ cm

distance from the shock interface to the cross section where a value of electron density of approximagely 3×10^{10} e/cc is obtained. For the case of these two pictures, the critical electron density is essentially the same as the equilibrium electron density. Hence the penetration distance may be related to the characteristic ionization relaxation distance. For Fig. III.4b the equilibrium electron density is slightly above critical; the measured distance is 1.6 centimeters. For Fig. III.4a the density is approximately critical and the measurement distance is 4 centimeters.

B. Generation of an Axially Nonuniform Plasma

The general procedure for obtaining an axially nonuniform plasma was described in Ref. (1). The specific experimental arrangement is discussed below.

The driven section of the shock tube is uniformly heated from the diaphragm section up to the transition region (see Fig. III.5). The heating elements are made by winding nichrome wire on top of thermal setting glass tape wound on the tube. All of the heated sections of the tube are insulated. The temperature in the transition region is controlled by several variable pitch heater sections. The temperature is measured by 24 thermocouples located on the outer surface of the tube. However, since the tube is relatively thin compared with the characteristic transition length, the temperature measured is essentially the temperature of the inner wall surface. An experiment has been performed to ascertain the relation between the gas temperature and the wall temperature for a change of $200^{\circ}C$ in one meter.
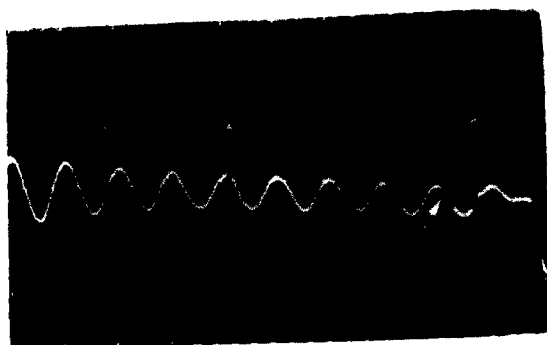
Figure III 4a

Uniform Plasma

Shock velocity 3400 m/s

Approx. SWR 2.0

$\lambda_g = 18.0$ cm

Marker interval 60 μ sec
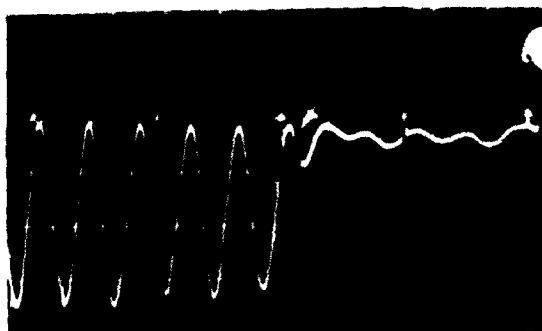
White arrow - blanking marker

Figure III 4b

Uniform Plasma

Shock velocity 3600 m/s

Approx. SWR 14

$\lambda_g = 18.0$ cm

Marker interval 60 μ sec

White arrow - blanking marker

In the range of pressure of .001 atm, the radial and longitudinal difference in temperature between local gas temperature and wall temperature is less than $1.5^{\circ}C$, in the center of the transition region. Near the ends of the transition, this difference was less than $10^{\circ}C$. Fig. III. 5c represents the temperature distribution for a transition length of 1 meter.

C. Measurements in Nonuniform Plasmas - CASE I

Using the method outlined in the previous section to generate a non-uniform plasma, the electromagnetic propagation into such a plasma has been experimentally examined for two gradient conditions in the driven section. For Case I, the transition length as defined above was 1.5 meters. Typically, this would produce a plasma where the electron density at the first shock interface could be $2x10^9$ e/cc increasing to $5x10^{10}$ e/cc in a length of about 15 cm. Such an electron density gradient is similar to that measured for argon (Refs. 2 and 3). Using the same analysis as in Ref. (2), the last maximum of the magnetic field trace corresponds to a value of electron density such that:

$$1 - \left(\frac{\omega_p}{ck_o}\right)^2 = 0$$

where,

$$\omega_p = 5.64x10^4 \sqrt{n_e}$$

$$k_o = 2\pi/\lambda_g$$

and λ_g = waveguide wavelength.

For $\lambda_g = 18.05$ cm (condition for plotted data)

$$n_e = 3x10^{10} \text{ e/cc.}$$

Transition
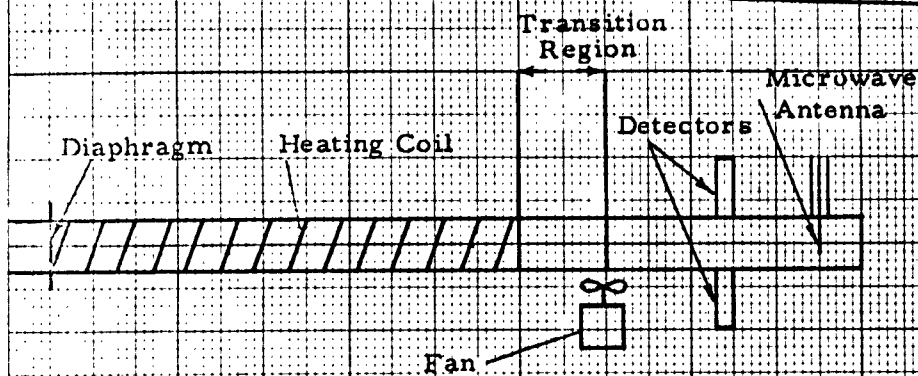Region

Microwave
Antenna

Detectors

Diaphragm   Heating Coil

Fan

Fig. III. 5a   Geometric arrangement of shock tube facility to generate
                 an axially nonuniform plasma.

°K Temperature

475

300

Diaphragm   Distance along tube
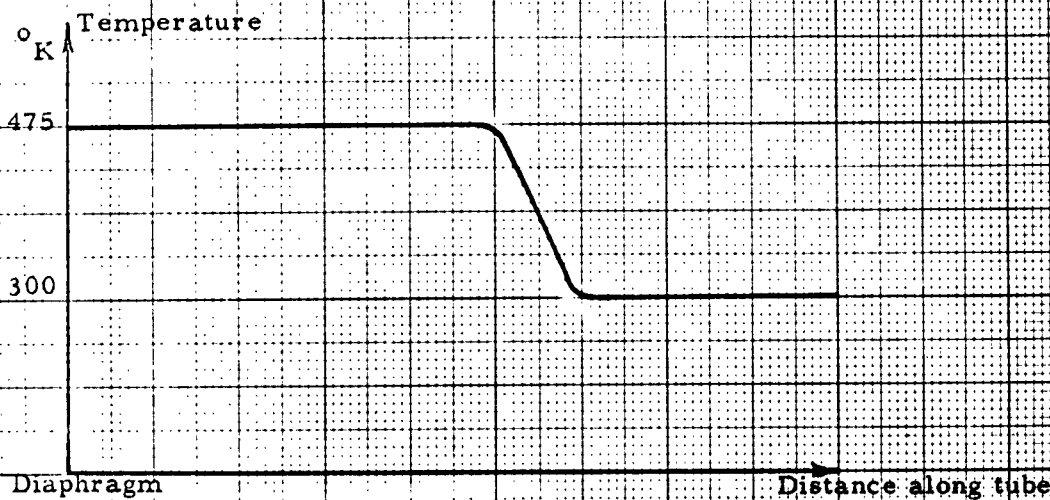
Fig. III. 5b   External Shock Tube Temperature - Case I Gradient

°K Temperature

475

300   Distance along tube
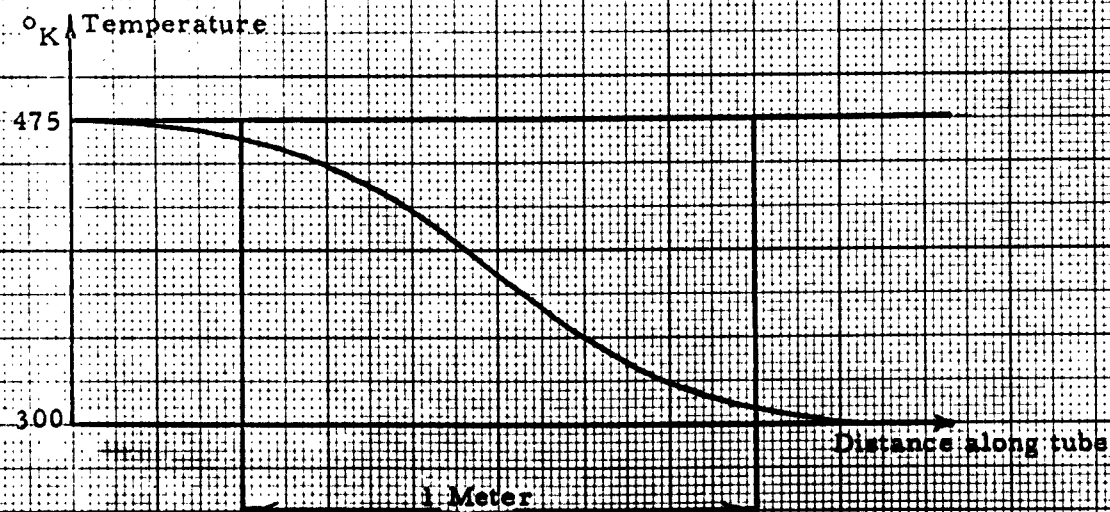
1 Meter

Fig. III. 5c   Estimated Internal Gas Temperature in the Transition Region
               for Case I Gradient.

Figure III. 6 diagramatically represents the electron density distribution for Case I behind the shock interface for different shock velocities. The distance behind the shock at which the critical electron density is attained increases as the shock velocity is decreased. Fig. III. 7 represents three typical magnetic field traces for different shock velocities, for the Case I plasma. The start of the blank trace is the location where the shock front is coincident with the magnetic field detector. From these measurements the curve in Fig. III. 8 has been obtained.

In the interpretation of these pictures, it should be clearly understood that the measured velocity is the velocity of the region where the transition from below to above critical electron density occurs. Only for the highest velocity case does the observed velocity approach the shock velocity. This occurs when the initial jump in electron density at the front of the shock exceeds the critical value.

For the low velocity range in Fig. III. 8, the plasma is becoming transparent to the microwave radiation. From Fig. III. 8 it appears the velocity at which the plasma becomes transparent is 2200 m/sec. This velocity should be compared with the interface velocity between region 1 and 2 (as defined in Section II -A) when the electron density in region 2 is just critical. This velocity as calculated by the method in Section II-A is 2300 m/sec.
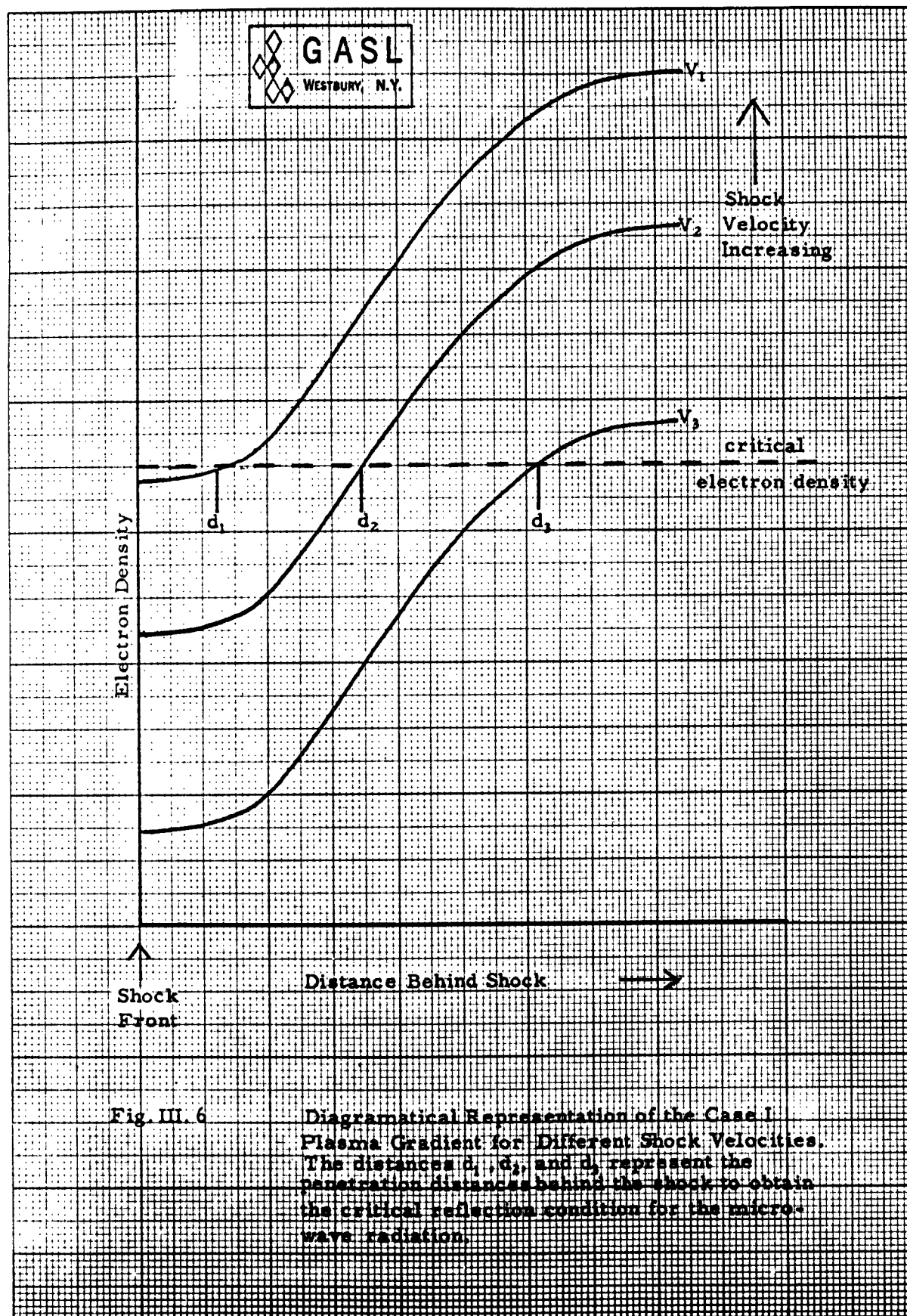
Fig. III. 6   Diagramatical Representation of the Case I Plasma Gradient for Different Shock Velocities. The distances d_1, d_2, and d_3 represent the penetration distances behind the shock to obtain the critical reflection condition for the micro-wave radiation
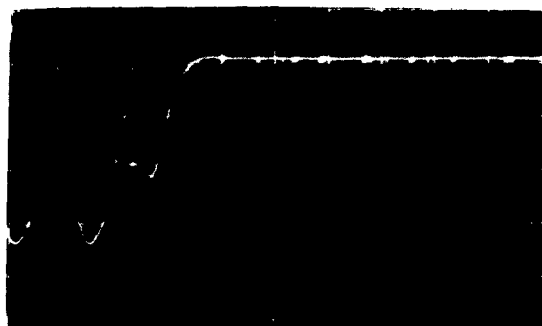
Case I gradient

Apparent shock velocity 3700 m/s

$\lambda_g = 18.$ cm

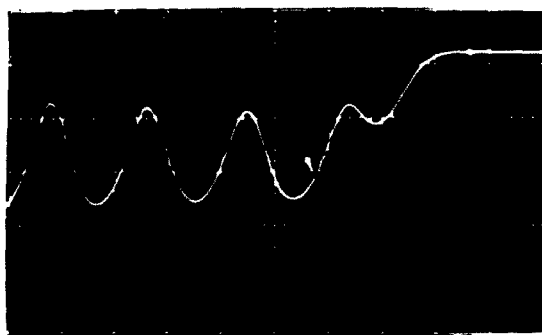Marker interval 60 μ sec

White arrow - blanking marker

Figure III 7a

Apparent shock velocity 2850 m/s

Figure III 7b
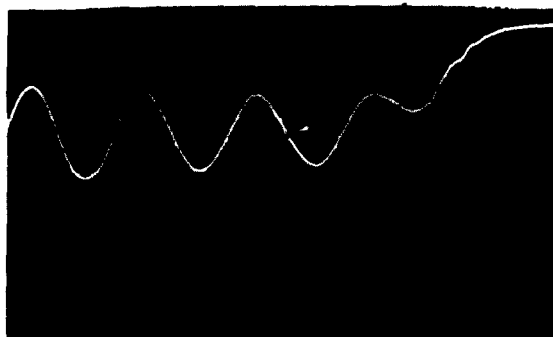

Apparent shock velocity 2300 m/s

Figure III 7c

Fig. III-8 Distance from shock front to H-max vs apparent shock velocity

Apparent Shock Velocity (meter/sec)

Distance from shock front to H-max (cm)

NO. 340R-20 DIETZGEN GRAPH PAPER
20 X 20 PER INCH

EUGENE DIETZGEN CO.
MADE IN U. S. A.

GASL
WESTBURY, N.Y.

D. Measurements in a Nonuniform Plasma - Case II

The temperature distribution along the driven tube to produce the Case II gradient is shown in Fig. III.9 along with the estimated internal gas temperature distribution. This Case II should approach the step change in temperature assumed for the calculation of shock properties in Section II.A. From the temperature and gas densities calculated from this ideal step transition, the equilibrium electron density in the regions behind the incident shock are plotted against the shock velocity prior to the arrival of the shock at the temperature discontinuity in Fig. III.10 and Fig. III.11. The two figures are for two driven pressures typical of the experimental conditions. From the experimental curve of shock velocity (prior to temperature transition) vs. initial pressure, Fig. III.12, the ideal electron density profiles in the axial direction can be ascertained for the actual operating conditions. Using the values of electron density and collision frequency as determined above, the system of equations outlined in Section II.C can be solved.

The results of the electromagnetic calculation can be presented in terms of the reflected power. This information is plotted in Fig. III.13 where the calculation is started at the temperature transition and proceeds for two meters (location of detectors) duplicating the actual experimental conditions.
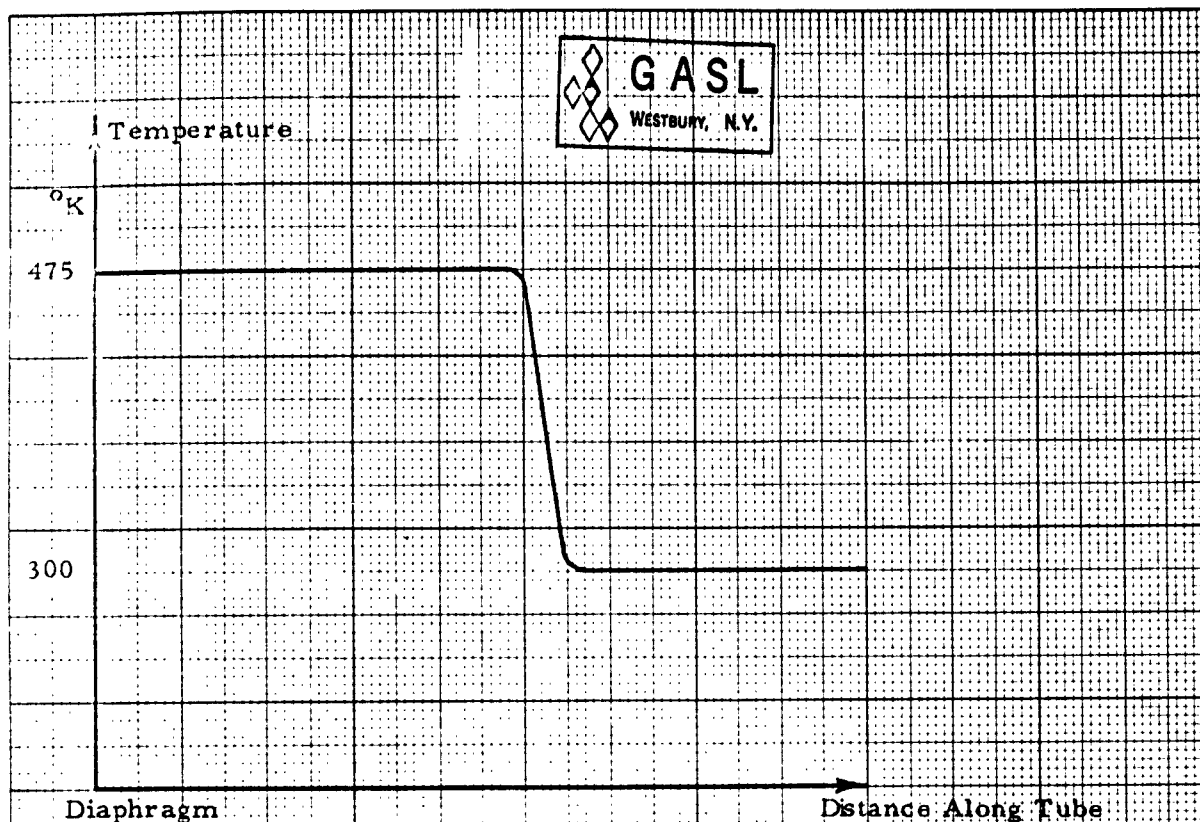
Figure III. 9a   External Shock Tube Temperature
Case II Gradient
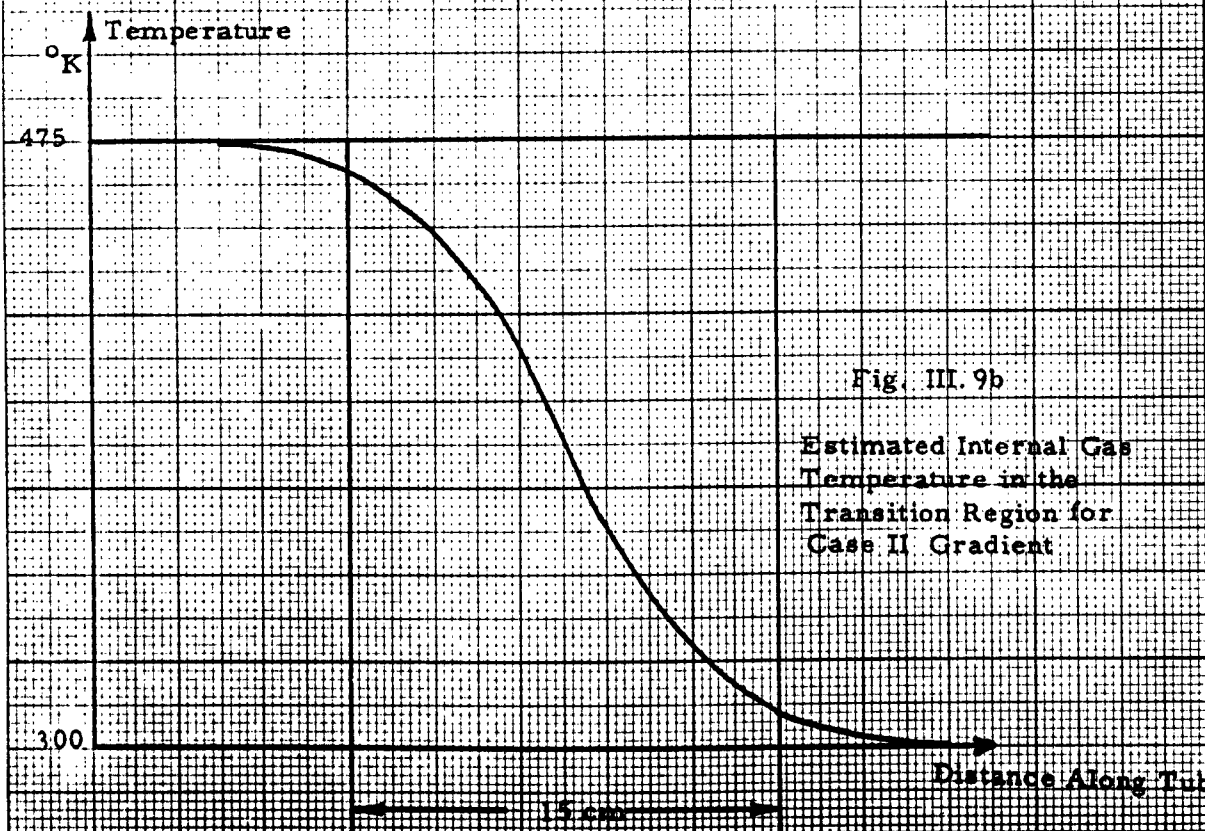
Fig. III. 9b

Estimated Internal Gas
Temperature in the
Transition Region for
Case II Gradient

Figure III.10   Computed Electron Density in
Regions 1, 2 and 3 (as defined in
Section II-B)

vs: Shock Velocity prior to Transition
for a Constant Initial Driven
pressure of .5x10^{-3} atm.

Electron Density (e/cc)

Shock Velocity Prior to Transition Region (meters/sec)

Fig. III.11

Computed Electron Density in regions 1, 2 and 3 (as defined in Section II-B) vs. shock velocity prior to transition for a constant initial driven pressure of 2.5×10^{-3} atm.

Shock Velocity Prior to Transition Region (meters/sec)
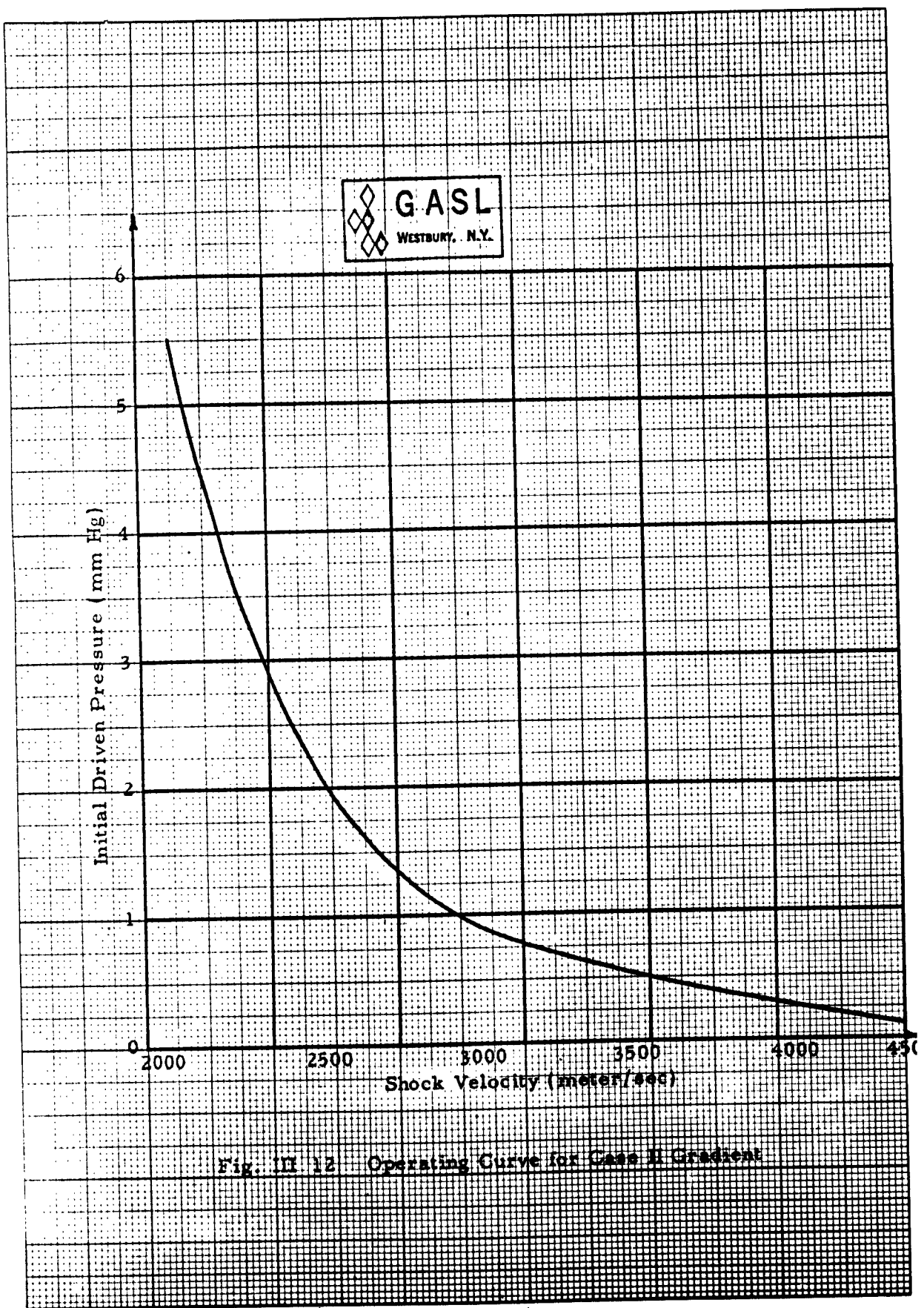
Electron Density (e/cc)
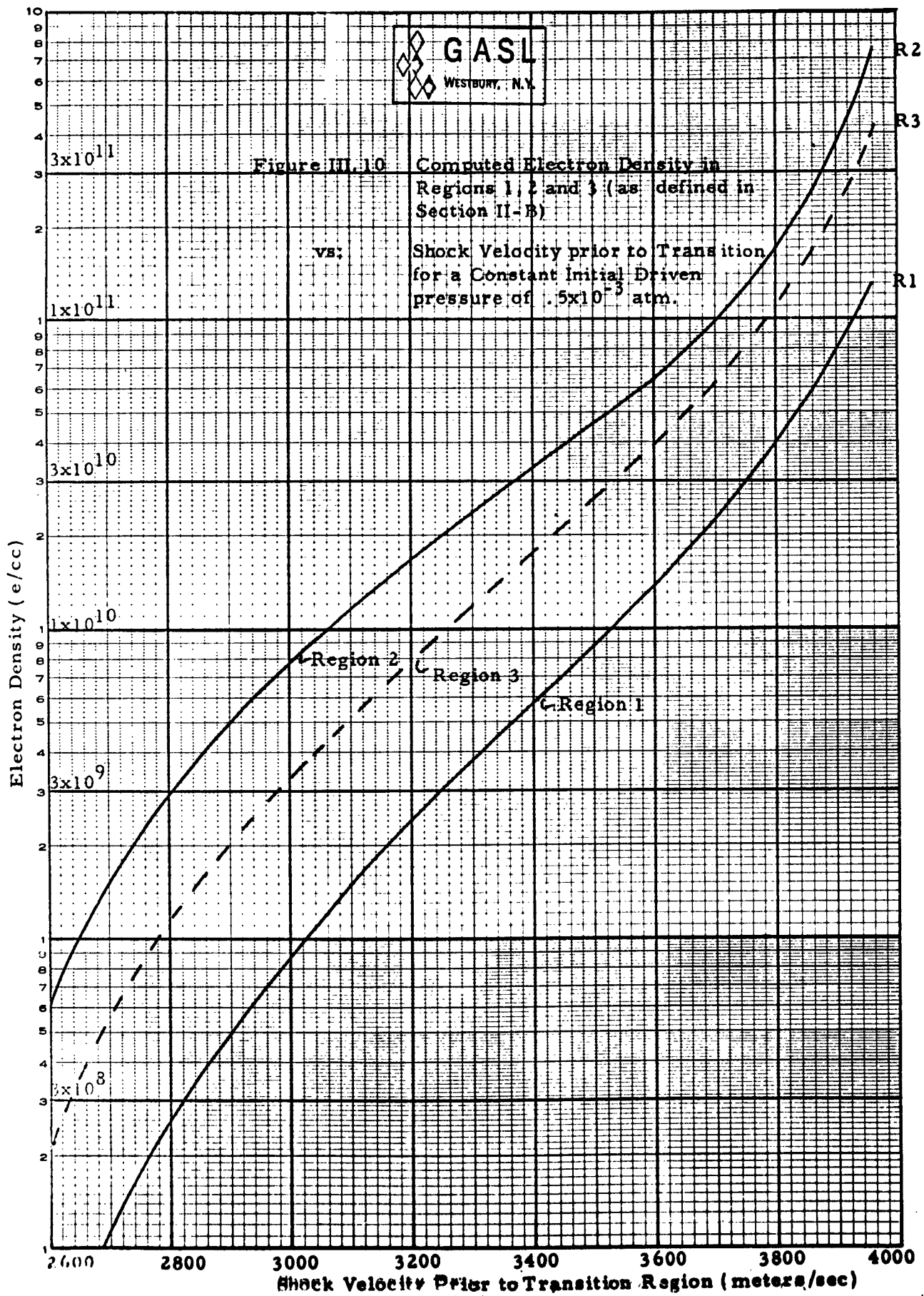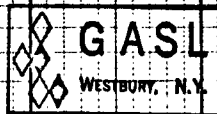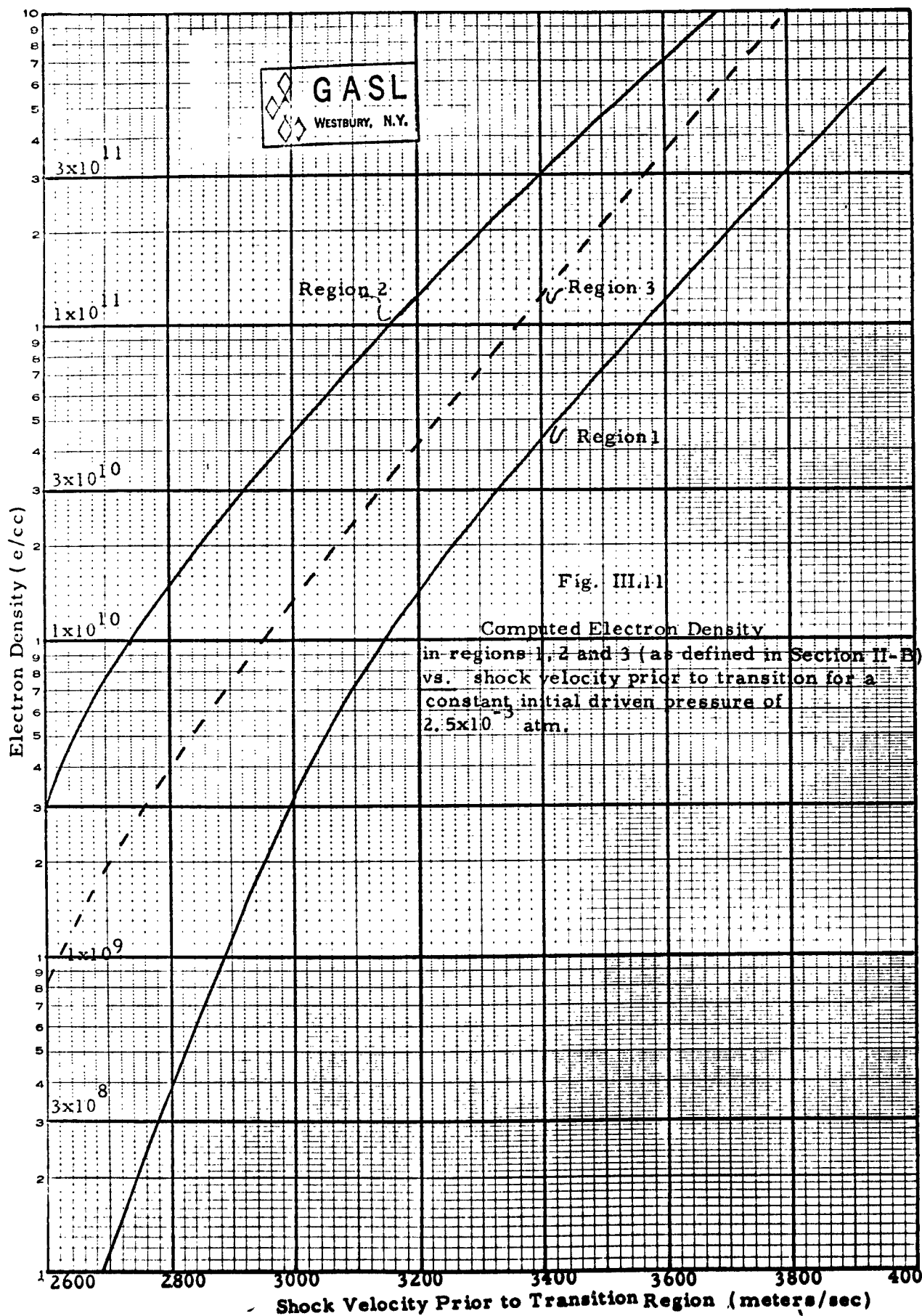
Fig. II 12   Operating Curve for Case II Gradient

Three pictures for incident shock velocities in the range of the theo-
retical curves of Fig. III.13 are presented in Figs. III.14, III.15, and III.16.
As the shock traverses the transition region the measured velocity change is
in good agreement with the aerodynamic calculations made in Section II.A.
The change in standing wave ratio as observed in Fig. III.14 corresponds to
the predicted SWR for curve a) of Fig. III.13. Similarly the increase in
SWR just after the transition is clearly evident from Figs. III.15 and III.16,
corresponding to curves b,c of Fig. III.13. However, for the latter experi-
mental curves, there is no apparent modulation as predicted by the calcula-
tion. This modulation should be a direct consequence of the fact that some
power is reflected from both the shock front and the interface between
regions (1) and (2). For the case wherein region (1) the electron
density is just below the critical value (curve b),this modulation should be
clearly evident and the period should be related to the difference in velocities
of the two interfaces.

Another observed difference between the experiment and the ideal
calculations is that in Fig. III.15, some evidence of wave propagation should
be found in region (1) since for this shock condition, the electron density in
region (1) is slightly below critical. Experimentally the electric field is
observed to decay rapidly inside region (1).

SWR

$V_i = 3790$ m/s

$V_i = 3330$ m/s

$V_i = 2850$ m/s

Time from contemperature Transition   μ sec

100   200   300   400   500   600   700
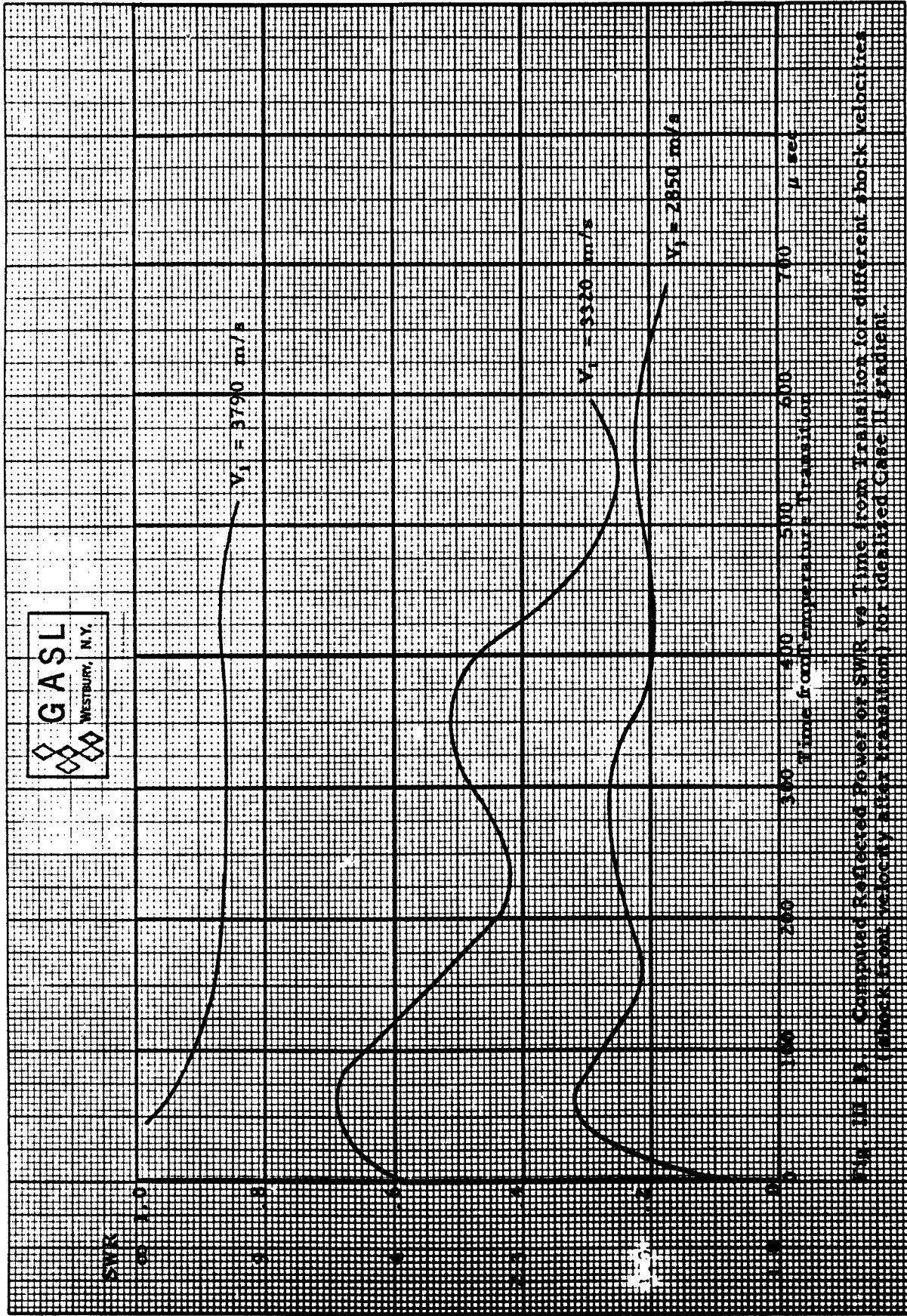
GASL
WESTBURY, N.Y.

Fig. 18-13: Computed Reflected Power of SWR vs time from transition for different shock velocities (shock front velocity after transition) for Idealized Case III gradient.
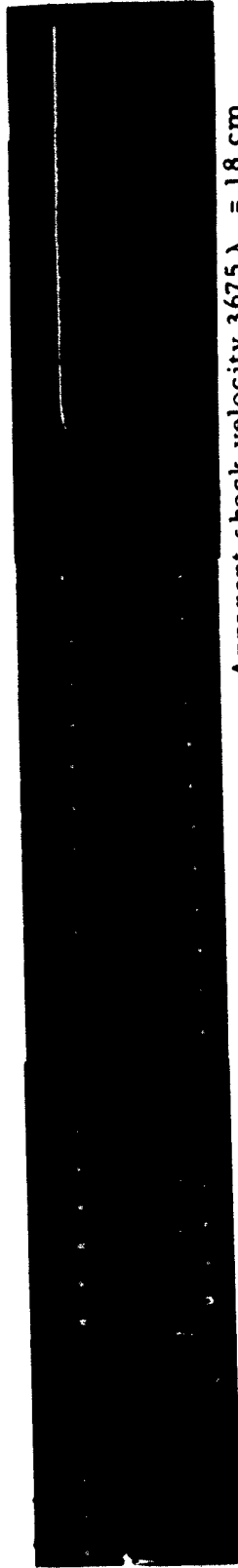
Figure III 14   Case II gradient
(Composite scope picture)

Apparent shock velocity 3675 λ_g = 18 cm
marker 60 μ sec interval
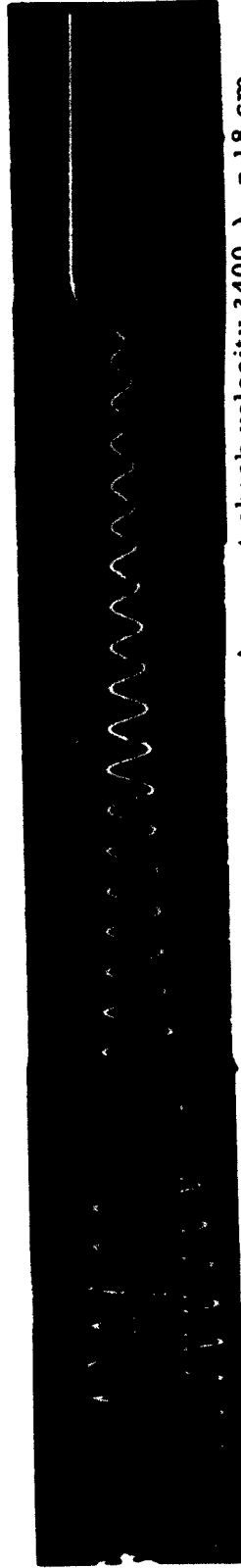
Figure III 15   Case II gradient
(Composite scope picture)

Apparent shock velocity 3400 λ_g = 18 cm
marker 60 μ sec interval

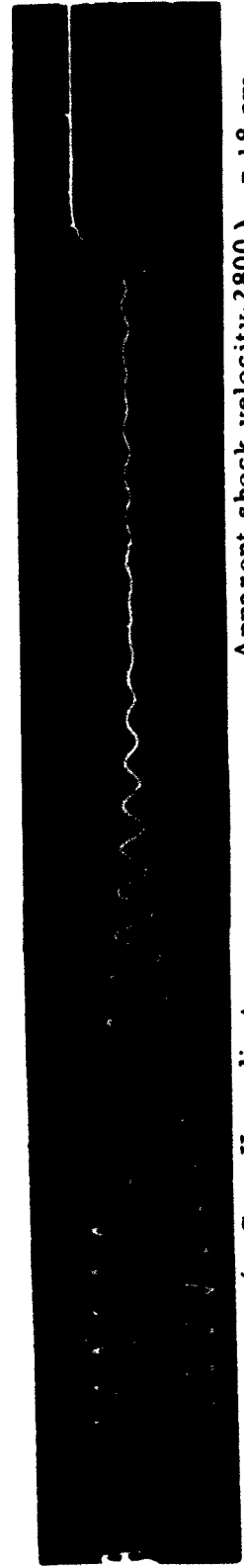Figure III 16   Case II gradient
(Composite scope picture)

Apparent shock velocity 2800 λ_g = 18 cm
marker 60 μ sec interval

Additional experiments were made with the initial pressure in the driven section an order of magnitude below that used in the tests discussed above. The combination of increased velocity and decreased density produced the same range of electron densities as those produced in the higher pressure cases. For the low pressure cases, some evidence of propagation inside region (1) was observed.

E. Improvement in the electric and Magnetic Field Detectors

The electric field detector is basically a resonant coaxial line, capacitively coupled to the waveguide at the open end and with the crystal detector connected between center and outer conductor at $\frac{\lambda}{2}$ from the open end. The center conductor is flush mounted with respect to the inner surface of the tube (see Fig. III. 17a). The coupling can be modified by changing the size of the washer located at the end of the center conductor. The system is tuned with a sliding short-circuit.

The magnetic field detector consists of a slot normal to the current flow in the wall of the tube. The signal induced between the two sides of the slot, excites a two-conductor resonant line. A crystal detector is connected between the conductors (see Fig. III. 17b).

In both detectors the main improvements are:

a) no aerodynamic perturbations

b) larger output and, at the same time, better signal to noise ratio because of the resonant circuits.

Characteristic values for the output are .5 volts. In order to eliminate the phase difference between the two signals, both detectors have been mounted

in the same transversal section of the tube. Provision has been made to locate

in the same plane of the microwave detectors either a pressure gage or an

ionization gage so as to correlate microwave signals with the shock interface

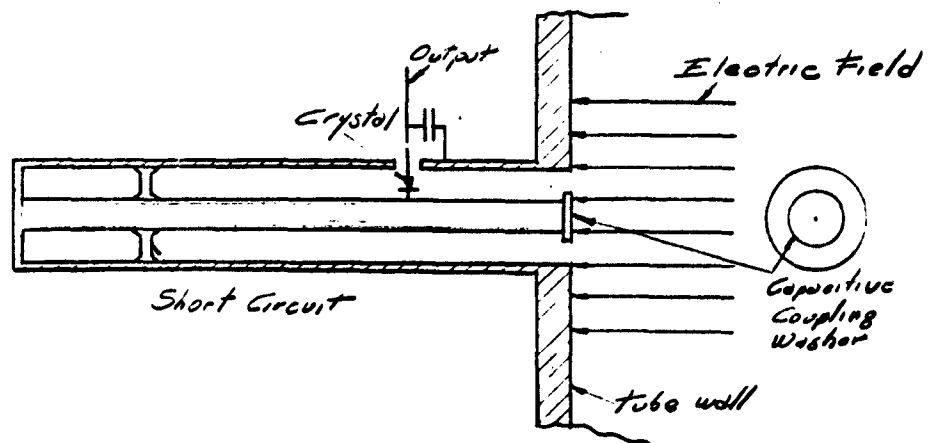position.

Electric Field Detector

Output

Crystal

Electric Field

Short Circuit

Capacitive Coupling Washer

tube wall

Figure III 17a

Magnetic Field Detector

Output

Crystal

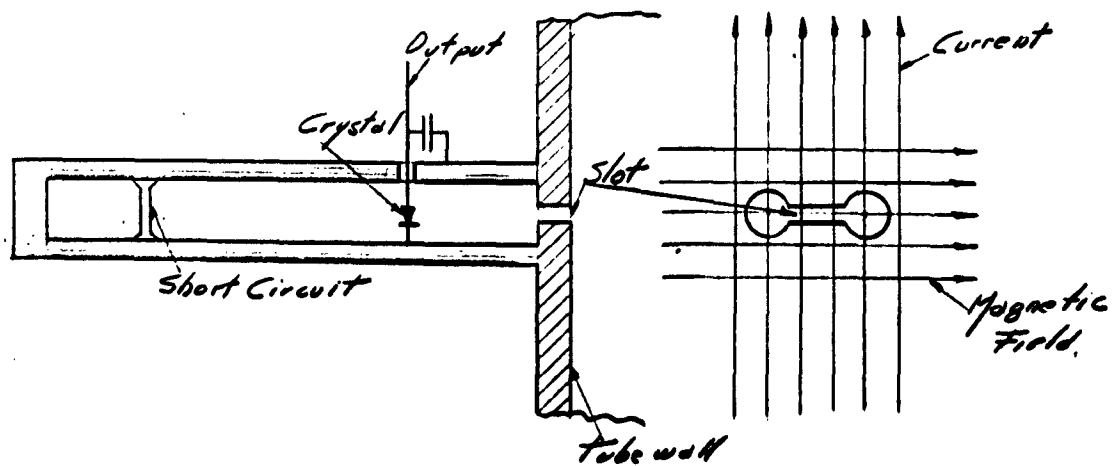Current

Slot

Short Circuit

Magnetic Field

Tube wall

Figure II 17b

IV. CONCLUDING REMARKS

This semi-annual technical summary report presents the initial series of electromagnetic measurements in a nonuniform air plasma. In the range of measurements conducted thus far the beginning of the transient process in the electron distribution behind the shock interface is clearly shown in the signals from the microwave detectors. The change of shock velocity in the transition region is in good agreement with the preliminary theoretical analysis of the flow field.

The measured ionization relaxation lengths are of the order of several centimeters in the present range of experimental conditions. The range of equilibrium electron densities appears to be in good agreement with the expect theoretical values. The absorption of the microwave signal in the plasma region appears, for some cases, to be exceedingly high compared with the theoretical values obtained on the basis of the simple uniform plasma model used in the theoretical calculations.

REFERENCES

1. Abele, M., Napolitano, L., Caldirola, P., Lane, F., Tomboulian, R., Wecker, M., Moretti, G., GASL TR-255, First Semi-Ann'l. Tech. Repor Studies of the Electromagnetic Characteristics of Moving Ionized Gases, Oct. 31, 1961.

2. Napolitano, L., Wecker, M., Medecki, H., Abele, M., Calfirola, P., Tomboulian, R., Gavril, B., GASL TR-290, Second Semi-Ann'l. Tech. Summary Report, Studies of the Electromagnetic Characteristics of Movin; Ionized Gases, April 30, 1962.

3. Gavril, B., Abele, M., Albertoni, S., Cercignani, C., Tomboulian, R., Mariano, S., GASL TR-316, Third Semi-Ann'l. Tech. Summary Report, Studies of Electromagnetic Properties of Nonuniform Plasmas, Oct. 1, 1962.

4. Courant, R., and Friedrichs, K.O., Supersonic Flow and Shock Waves, Interscience Publishers, Inc., New York

5. Moretti, G., and Tamagno, J., Study of a Shock-Tube Attachment to Simulate the Shock Layer Past an I.C.B.M. Flying at very high Altitudes, GASL TR-189.

6. Moretti, G., Analytical Expressions for a Speedy Computation of the Thermodynamical Properties of Air, GASL TR-39, Nov. 1960.